Correcting errors in a quantum gate with pushed ions via optimal control

Uffe V. Poulsen
Lundbeck Foundation Theoretical Center for Quantum System Research, Department of Physics and Astronomy, Aarhus University, DK 8000 Aarhus C, Denmark

Shlomo Sklarz and David Tannor
Department of Chemical Physics, Weizmann Institute of Science, 76100 Rehovot, Israel

Tommaso Calarco
Institut für Quanteninformationsverarbeitung, Albert-Einstein-Allee 11, D-89069 Ulm, Germany and European Centre for Theoretical Studies in Nuclear Physics and Related Areas, I-38050 Villazzano, Italy

(Received 26 October 2009; revised manuscript received 8 June 2010; published 30 July 2010)

We analyze in detail the so-called pushing gate for trapped ions, introducing a time-dependent harmonic approximation for the external motion. We show how to extract the average fidelity for the gate from the resulting semiclassical simulations. We characterize and quantify precisely all types of errors coming from the quantum dynamics and reveal that slight nonlinearities in the ion-pushing force can have a dramatic effect on the adiabaticity of gate operation. By means of quantum optimal control techniques, we show how to suppress each of the resulting gate errors in order to reach a high fidelity compatible with scalable fault-tolerant quantum computing.

DOI: 10.1103/PhysRevA.82.012339 PACS number(s): 03.67.Lx, 02.30.Yy

I. INTRODUCTION

Trapped ultracold ions have represented a major candidate for the implementation of scalable quantum information processing since the beginning of this research field. The first proposal of an ion-based quantum computer by Cirac and Zoller in 1995 [1] has been followed by a great variety of other schemes based on ions [2], on other quantum optical systems like neutral atoms [3,4], and on solid-state systems [5]. With the progress in experimental techniques and the demonstration of entangling quantum gates based on several different candidate physical systems, the focus has progressively shifted toward the fulfillment of scalability desiderata [6], that is, the realization of quantum gates with very high fidelities, in the range 0.999–0.9999.

Gate errors in a real implementation of a given quantum gate scheme can be reduced by different means. Some errors arise from (or are increased by) experimental imprecisions of a technical nature and can be controlled by careful alignment, stabilization, and so on, of the experimental apparatus. Other errors stem from unaviodable interactions with the environment and can be reduced simply by completing the gate in as short a time as possible. Typically, a gate scheme can be made faster by simple scaling to higher intensities, shorter distances, and so on. If such simple optimizations of the gate prove insufficient, one needs to consider changes to the scheme itself and trade simplicity for improved performance. This is exactly the goal of quantum optimal control techniques [7], which allow for a precise tailoring of the system's evolution by time-dependent tuning of some external parameters. With sufficient control over these parameters, a given target state can often be reached with minimal error even over short gate operation times. The application of these methods to quantum information systems requires in turn a very accurate simulation of the dynamics and a careful understanding of the targeted error sources. This is precisely the aim of this article, in the specific case of the two-qubit ion gate proposed in [2] and subsequently analyzed in [8,9]. In this pushing gate, the qubits are encoded in the internal states of two ions. Each ion is held in a separate microtrap and state-selective push potentials are applied in order to modify the distance and thus the Coulomb interaction between ions (see Sec. III). We shall first point out a series of issues that arise when the assumption of spatial homogeneity of the ion-driving force is dropped and subsequently develop a way to correct each of these issues, exploting a range of ideas, including in a crucial way optimal control methods.

It should be noted from the outset that in the present article, we analyze the pushing gate without what is called the π-pulse method in Refs. [8,9], where it was shown to dramatically reduce some types of errors. The π-pulse method is a spin-echo technique and requires the gate to be repeated with the internal state of the ions flipped. Typically, single-particle operations like flipping the internal states can be done with high fidelity, and it is reasonable to expect that eventually, the π-pulse method will be used. However, internal state control is at least in principle a separate issue from the pushing gate operation itself. Keeping the design process modular in spirit, it is relevant to optimize the gate without this additional trick and thus pave an alternative road to high fidelities. As will become clear, we extract quite general noise-reduction methods from the automated numerical optimization results, and it is an interesting topic for future research to combine these with the π-pulse method.

The remainder of the article is organized as follows. In Sec. II, we introduce the general setting of conditional dynamics gate schemes, a useful approximation for simulating such a gate, and a measure of the gate errors. In Sec. III, we specialize to the pushing gate. The unoptimized performance of the gate is reported in Sec. IV, and in Sec. V, we show how this performance can be significantly improved by a combination of manual changes and numerical optimal control methods. Finally, we conclude in Sec. VI. Appendix A–C contains a number of more technical results and derivations.

II. CONDITIONAL DYNAMICS

The basic idea of the so-called pushing gate is one of conditional dynamics; that is, we apply potentials depending on the internal state of the two ions. The internal states themselves are not changed during the gate, or in the case of the π-pulse method, are changed on a much shorter time scale than the external dynamics. This means that the analysis of the problem splits into four separate evolutions for the external state, one for each of the logical (internal) states 00, 01, 10, and 11. In the following, these four evolutions will be denoted as "branches" and will be indexed by $\beta \in \{00,01,10,11\}$. The complete Hamiltonian can be written in the form of a sum of internal $\otimes$ external factorized terms

$$\hat{H}^{\mathrm{tot}}(t) = \sum_{\beta} |\beta\rangle\langle\beta| \otimes \hat{H}^{\mathrm{ex}}_{\beta}(t), \tag{1}$$

and it results in an evolution operator of a similar form:

$$\hat{U}^{\mathrm{tot}}(t) = \sum_{\beta} |\beta\rangle\langle\beta| \otimes \hat{U}^{\mathrm{ex}}_{\beta}(t). \tag{2}$$

Ideally, when $t = T$ at the end of the gate, the U^{ex}_{β} should differ from each other by at most a phase factor multiplying a common unitary operator $\hat{U}^{\mathrm{ex}}_{\mathrm{com}}$:

$$\hat{U}^{\mathrm{ex}}_{\beta}(T) = e^{i\theta_{\beta}} \hat{U}^{\mathrm{ex}}_{\mathrm{com}} \tag{3}$$

so that $\hat{U}^{\mathrm{tot}}$ itself can be factorized:

$$\hat{U}^{\mathrm{tot}}(T) = \left(\sum_{\beta} |\beta\rangle\langle\beta| e^{i\theta_{\beta}} \right) \otimes \hat{U}^{\mathrm{ex}}_{\mathrm{com}}. \tag{4}$$

The internal evolution is then that of a phase gate, while the external evolution can in principle be undone using internal-state-independent potentials.

The requirement (3) is very hard to achieve and would make the gate completely independent on the initial external state. However, we can typically assume to have some degree of control over the initial external state, for example, by cooling the particles before the gate. This means that Eq. (3) need only hold when restricted to a subset of the complete Hilbert space, typically the states of relatively low energy. In Appendix B, we show how to evaluate the performance of the gate in general. For now, we note that since only the low-energy part of $\hat{U}^{\mathrm{ex}}_{\beta}(T)$ will be important, we can focus on getting a good approximation for this part when trying to simulate the gate dynamics.

A low initial energy means particles localized near the potential minimum, and this suggests using a harmonic approximation to the real potential.[1] The simplest choice is to Taylor expand around a fixed point, which is not changed during the gate operation. The next level of refinement is to expand around the instantaneous potential minimum. This works very well if the gate operation is nearly adiabatic so the particles stay near the (moving) minimum at all times. However, it may be desirable to make fast and substantial changes to the potential during the gate, and that may induce pronounced nonadiabatic dynamics. In that case, the harmonic approximation can still be a good one, provided it is done around the classical trajectories of the particles. Typically these trajectories cannot be computed analytically, but for any moderate number of particles, it is a numerically simple task to find them. In the following, we will use this method and show how it leads to a relatively simple characterization of U^{ex}_{β}.

A. Harmonic approximation

In this section, we focus on a single branch of the evolution and thus suppress the β index. Let us denote by $\bar{\mathbf{x}}(t)$ the classical trajectory, which is found by solving classical equations of motion. The time-dependent, second-order Taylor expansion of the potential $V(t,\mathbf{x})$ around $\bar{\mathbf{x}}(t)$ reads simply

$$V_{\mathrm{so}}(t,\mathbf{x}) = V^{(0)}(t) + \Delta\mathbf{x}^{\mathrm{T}}\mathbf{V}^{(1)}(t) + \tfrac{1}{2}\Delta\mathbf{x}^{\mathrm{T}}V^{(2)}(t)\Delta\mathbf{x}, \tag{5}$$

with $\Delta\mathbf{x} = [\mathbf{x} - \bar{\mathbf{x}}(t)]$ and

$$\begin{aligned} V^{(0)}(t) &= V(t,\bar{\mathbf{x}}), \\ V^{(1)}_i(t) &= \frac{\partial V}{\partial x_i}(t,\bar{\mathbf{x}}), \\ V^{(2)}_{ij}(t) &= \frac{\partial^2 V}{\partial x_i \partial x_j}(t,\bar{\mathbf{x}}). \end{aligned} \tag{6}$$

Note that we will still use $\mathbf{x}$ as our coordinate; that is, we are not changing to a coordinate system moving with $\bar{\mathbf{x}}(t)$. Rather, we simply use a potential that approximates the real potential close to $\bar{\mathbf{x}}(t)$. Collecting terms of equal order in $\mathbf{x}$ leads to the alternative form

$$V_{\mathrm{so}}(t,\mathbf{x}) = E(t) - \mathbf{x}^{\mathrm{T}}\mathbf{F}(t) + \tfrac{1}{2}\mathbf{x}^{\mathrm{T}}K(t)\mathbf{x}, \tag{7}$$

with

$$\begin{aligned} E(t) &= V^{(0)}(t) - \bar{\mathbf{x}}^{\mathrm{T}}(t)\mathbf{V}^{(1)}(t) + \tfrac{1}{2}\bar{\mathbf{x}}^{\mathrm{T}}(t)V^{(2)}(t)\bar{\mathbf{x}}(t), \\ \mathbf{F}(t) &= -\mathbf{V}^{(1)}(t) + V^{(2)}(t)\bar{\mathbf{x}}(t), \\ K(t) &= V^{(2)}(t). \end{aligned} \tag{8}$$

B. Gaussian evolution

The big advantage of choosing a second-order approximation to the real potential is that this restricts the corresponding approximate $\hat{U}^{\mathrm{ex}}(t)$ to be Gaussian for all t. Let us introduce the compact notation $\mathbf{q} = (\mathbf{x},\mathbf{p})$ and define the matrix J by

$$J = \begin{bmatrix} 0 & \mathbb{I}_n \\ -\mathbb{I}_n & 0 \end{bmatrix}, \tag{9}$$

where n is the number of degrees of freedom. Then the usual canonical commutation relations can be written as

$$[q_i, q_j] = i J_{ij}. \tag{10}$$

With the potential of Eq. (7) and a matrix of particle masses $M = \mathrm{diag}(m_1,\ldots,m_n)$, the time-dependent Hamiltonian becomes

$$\hat{H}_{\mathrm{so}} = \tfrac{1}{2}\hat{\mathbf{p}}^{\mathrm{T}}M^{-1}\hat{\mathbf{p}} + V_{\mathrm{so}}(t,\hat{\mathbf{x}}). \tag{11}$$

In Appendix A, we show that such a Hamiltonian leads to an evolution operator of the form

$$\hat{U}(t) = e^{-i\phi(t)}\hat{D}_{\mathbf{c}(t)}\hat{W}_{b(t)}, \tag{12}$$

[1] For a thorough introduction to semiclassical wave packet methods, see, e.g., Ref. [10].

where $\hat{D}_{\mathbf{c}}$ is a displacement operator and $\hat{W}_b$ is a squeezing operator:

$$\hat{D}_{\mathbf{c}} = e^{-i\mathbf{c}^{\mathrm{T}} J\hat{\mathbf{q}}},$$
$$\hat{W}_b = e^{-i\frac{1}{2}\hat{\mathbf{q}}^{\mathrm{T}} b\hat{\mathbf{q}}}. \tag{13}$$

The scalar ϕ, the vector $\mathbf{c}$, and the matrix $S = \exp(Jb)$ should satisfy the following equations of motion:

$$\frac{\partial}{\partial t}\phi = E - \frac{1}{2}\mathbf{F}^{\mathrm{T}}\bar{\mathbf{x}},$$
$$\frac{\partial}{\partial t}\mathbf{c} = Jh\mathbf{c} + \begin{bmatrix} 0 \\ \mathbf{F} \end{bmatrix}, \tag{14}$$
$$\frac{\partial}{\partial t}S = JhS,$$

where the $2n \times 2n$ matrix h is defined by

$$h(t) = \begin{bmatrix} K(t) & 0 \\ 0 & M^{-1} \end{bmatrix}. \tag{15}$$

The form of solution (12)–(14) holds for any second-order Hamiltonian. In the particular case where V_{so} is a Taylor expansion of a real potential around the classical trajectory $\bar{\mathbf{x}}(t)$, the equation of motion for $\mathbf{c}$ reduces to the exact equation of motion for $\bar{\mathbf{q}} = (\bar{\mathbf{x}}, \bar{\mathbf{p}})$ where $\bar{\mathbf{p}}$ is the classical momentum. In the following, we will therefore write $\bar{\mathbf{q}}$ instead of $\mathbf{c}$. It is then important to remember that the right-hand sides of Eqs. (14) are in general nonlinear functions of $\bar{\mathbf{x}}$.

C. Fidelity

We can quantify the performance of the gate by calculating the average fidelity F_{av} (see Appendix B) between the obtained output state and the ideal one when the input state is varied. One can then separate out three kinds of contributions to the deviation of F_{av} from 1 (the perfect gate):

$$1 - F_{\mathrm{av}} = E_\theta + E_{\bar{\mathbf{q}}} + E_S. \tag{16}$$

The three types of errors each have their physical interpretation. The most straightforward one pertains to the sloshing errors $E_{\bar{\mathbf{q}}}$, which correspond to a residual motion of the ions after the gate has been completed and the microtraps are again at rest. The phase errors E_θ are errors in the gate phase. Finally, the breathing errors E_S are induced by differences in the harmonic approximation parameters around the classical trajectory for different internal states. For example, in the case we consider, when the particles are pushed closer together, the second-order term in the Coulomb repulsion becomes larger [cf. Eq. (25)].

In our model, we assume that systematic, local phase errors can be undone. Then an explicit calculation in Appendix B shows that the phase errors are given by

$$E_\theta = \tfrac{1}{20}(\theta_{00} - \theta_{01} - \theta_{10} + \theta_{11} - \pi)^2, \tag{17}$$

with $\theta_\beta = -\phi_\beta + \mathrm{Tr}[b_\beta \gamma]$, where γ is the covariance matrix of the external state (see Sec. B3). Note the inclusion of the $\mathrm{Tr}[b_\beta\gamma]$ terms in the definition of θ_β: These terms correspond to phase contributions from average excitation energy in the traps and are therefore temperature dependent through γ. For our parameters, they are small.

The sloshing errors are given by

$$E_{\bar{\mathbf{q}}} = \frac{1}{20}\sum_{\alpha<\beta}(\bar{\mathbf{q}}_\alpha - \bar{\mathbf{q}}_\beta)^{\mathrm{T}}\gamma(\bar{\mathbf{q}}_\alpha - \bar{\mathbf{q}}_\beta), \tag{18}$$

and the breathing errors are

$$E_S = \frac{1}{40}\sum_{\alpha<\beta}\mathrm{Tr}[(b_\alpha - b_\beta)\gamma(b_\alpha - b_\beta)\gamma]$$
$$+ \frac{1}{160}\sum_{\alpha<\beta}\mathrm{Tr}[(b_\alpha - b_\beta)J(b_\alpha - b_\beta)J]. \tag{19}$$

Here ϕ_β, $\bar{\mathbf{q}}_\beta$, and b_β are defined in Eqs. (12) and (13) and are the variables describing the Gaussian approximation in the β branch of the evolution. Again, γ introduces temperature dependence.

III. THE PUSHING GATE

Let us now focus on the particular case of the pushing gate. Here we have two ions, each in a separate microtrap.[2] To further simplify the discussion, we concentrate on just one spatial dimension; that is, there are two degrees of freedom, $n = 2$. The ions are assumed to be of identical mass, $m_1 = m_2 = m$, and thus $M = m\mathbb{I}_2$. The potential energy consists of a microtrap for each ion, time- and internal state–dependent pushing potentials, and of the Coulomb interaction. The pushing potentials can be realized as optical dipole potentials generated by focused laser beams. The time dependence of these potentials is most easily achieved by controlling the intensity of the laser and the state selectivity by polarization selection rules [9]. We assume that the form for the internal state labeled by β is

$$V^{(\beta)}(t,\mathbf{x}) = \sum_{i=1,2}\frac{1}{2}m\omega^2 x_i^2 + \frac{e^2}{4\pi\epsilon_0\,|d + x_2 - x_1|}$$
$$+ \sum_{i=1,2} f_i^{(\beta)}(t)\frac{\hbar\omega}{a_0}\left[-(-1)^i x_i + \frac{G}{a_0}x_i^2\right]. \tag{20}$$

The trapping potentials are assumed to be perfectly harmonic. The state-dependent pushing amplitudes $f_i^{(\beta)}$ are such that the ions are only pushed if they are in the internal state 1, $f_i^{(\beta)}(t) = \delta_{\beta_i,1} f(t)$. Note that the $(-1)^i$ factor means that ion 1 is pushed to the left and ion 2 to the right. Nonlinear contributions to the pushing potentials are included via the constant G. The harmonic oscillator ground-state size is $a_0 = \sqrt{\hbar/m\omega}$. The two coordinates x_1 and x_2 are taken to have origins in the respective trap centers, a distance d apart. Experimentally, the parameters in Eq. (20) can be varied quite a lot (see, e.g., [9]). Trap distances d from 100 μm all the way down to 1 μm are within technological reach. The trap frequency ω can be chosen in the range $2\pi \times (10^4$–$10^7)$ Hz, which for, for example, Ca^+ ions will mean an oscillator length a_0 from 150 down to 5 nm.

It should be noted that the use of optical dipole potentials to generate the state-selective pushing forces will in general

[2]The gate can also be implemented in a string of ions (see [8]) and treated by the method described in this article, but we focus exclusively on the two-ion case.

introduce large single-qubit phases because of ac Stark shifts. This is not a problem as such, but it means that even small fluctuations in laser intensities will lead to loss of gate fidelity. For the particular case of the pushing gate, the ac Stark shifts can be balanced against the Coulomb energy as discussed in Ref. [9]. Obviously ac Stark shifts are common to many gate proposals that use optical potentials. An experimentally demanding but quite general solution is to compensate the shifts along the lines of Refs. [11,12]. In this article, we focus on errors that are more directly related to the motion of the ions and assume that the push potentials are effectively nonfluctuating.

A. Dimensionless Hamiltonian

The relative strength of the Coulomb interaction to the trapping potentials turns out to be conveniently quantified by

$$\epsilon = \frac{\frac{e^2}{\pi\epsilon_0 d}}{m\omega^2 d^2} = \frac{a_0^2}{d^2}\frac{\frac{e^2}{\pi\epsilon_0 d}}{\hbar\omega}, \tag{21}$$

which is the ratio of the energy scale of the Coulomb and trap potential energies at the equilibrium positions of the ions. In Ref. [9], it was found that $\epsilon \ll 1$ is the most promising regime. In oscillator units, the Hamiltonian for the branch labeled by β reads

$$\hat{H}^{(\beta)}_{\text{push}}(t) = \sum_{i=1,2}\frac{1}{2}\left[\hat{p}_i^2 + \hat{x}_i^2\right] + \frac{\epsilon}{4}\frac{\frac{d^2}{a_0^2}}{\left|1+\frac{a_0}{d}(\hat{x}_2-\hat{x}_1)\right|} - \sum_{i=1,2} f_i^{(\beta)}(t)\left[\hat{x}_i + G\hat{x}_i^2\right]. \tag{22}$$

B. Harmonic approximation

When Eqs. (8) are specialized to the pushing gate, we get the following:

$$E^{(\beta)}(t) = \frac{1}{4}\epsilon\frac{a_0}{d}\left\{\frac{\bar{x}_2^{(\beta)}-\bar{x}_1^{(\beta)}}{1+\frac{a_0}{d}\left[\bar{x}_2^{(\beta)}-\bar{x}_1^{(\beta)}\right]}\right\}^3, \tag{23}$$

$$F_i^{(\beta)}(t) = -(-1)^i f_i^{(\beta)}(t) \mp \frac{1}{4}\epsilon\frac{d}{a_0}\frac{1+3\frac{a_0}{d}\left[\bar{x}_2^{(\beta)}-\bar{x}_1^{(\beta)}\right]}{\left\{1+\frac{a_0}{d}\left[\bar{x}_2^{(\beta)}-\bar{x}_1^{(\beta)}\right]\right\}^3}, \tag{24}$$

$$K_{ii}^{(\beta)}(t) = 1 + 2f_i^{(\beta)}(t)G + \frac{1}{2}\epsilon\frac{1}{\left\{1+\frac{a_0}{d}\left[\bar{x}_2^{(\beta)}-\bar{x}_1^{(\beta)}\right]\right\}^3}, \tag{25}$$

$$K_{12}^{(\beta)}(t) = K_{21}^{(\beta)}(t) = -\frac{1}{2}\epsilon\frac{1}{\left\{1+\frac{a_0}{d}\left[\bar{x}_2^{(\beta)}-\bar{x}_1^{(\beta)}\right]\right\}^3}. \tag{26}$$

When these expressions are inserted into Eqs. (14) and (15), we are ready to simulate the gate.

IV. RESULTS OF SIMULATION

A. Choice of parameters

Even with the simplifications we have introduced, there are still a lot of parameters in the problem. The optimal working point will always be dependent on experimental considerations beyond the simplified model treated here. For a discussion of parameters and design decisions, see Ref. [9]. For concreteness, we have chosen to focus on a limited set of parameters. We first assume the individual ion traps to be very well separated and let $a_0/d = 0.001$ in all calculations. Likewise, we assume a reasonably low value for ϵ of 0.04. Such parameters would result from, for example, ^{40}Ca ions placed in microtraps with trapping frequencies of $\omega \sim 2\pi \times 5$ MHz and separated by a distance of ~ 7 μm. For the traveling wave configuration with beam waist w considered in Ref. [9], $G = 4(a_0/w)(w/2x_0 - 2x_0/w)$, where x_0 is the initial position of the ion relative to the beam center. For realistic focusing of the push beam, $w \sim 1$ μm, this suggests variation of the nonlinearity coefficient G between 0 and 3×10^{-2}. As the initial temporal shape of the push pulse, we choose a Gaussian $f(t) = \xi \exp(-t^2/\tau^2)$, where the amplitude ξ should be chosen to give a gate phase of π. A simple estimate (for $G = 0$) suggests that we choose [8]

$$\xi^2 = \frac{\pi}{\sqrt{\pi/8}\,\epsilon\sqrt{1+\epsilon/2}\,\omega\tau}. \tag{27}$$

The temporal width of the pulse, τ, should be within an order of magnitude from the trap period if we want a fast gate. We will mainly look at τ in the range 1–10 trap periods, which for the parameters quoted earlier results a maximum excursion because of the push in the range from $12a_0$ down to $3a_0$.

B. Phase errors

The choice of push amplitude expressed by Eq. (27) is not optimal. This can be seen in Fig. 1, where we plot E_θ as a function of G. Even for $G = 0$, the gate phase is not exactly π. For $\omega\tau = 3.5$, we see that a nonzero G can improve the gate phase. This is not surprising, but it is also not very useful, as we shall see later, that E_θ is in general easy to reduce. In Fig. 1, results for three different temperatures are plotted, but the dependence on temperature is completely negligible.

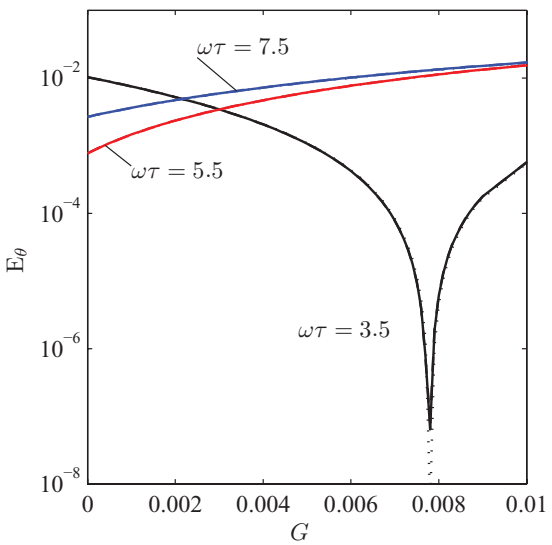

FIG. 1. (Color online) Phase errors with nonuniform pushing forces. The physical parameters are $\epsilon = 0.04$, $a_0/d = 0.001$, and $\omega\tau = 3.5$ (black), 5.5 (red), and 7.5 (blue). Results for temperatures of $T = (0.125, 1, 8) \times \hbar\omega/k_B$ are plotted for each value of τ and are indistinguishable from each other.

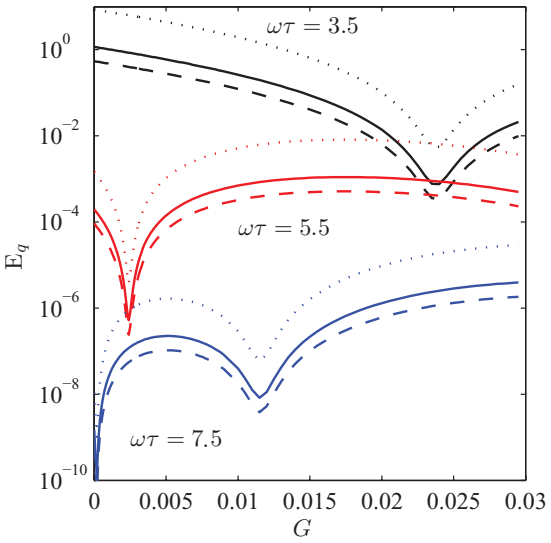

FIG. 2. (Color online) Sloshing errors with nonuniform pushing forces. The physical parameters are $\epsilon = 0.04$, $a_0/d = 0.001$, and $\omega\tau = 3.5$ (black), 5.5 (red), and 7.5 (blue). We plot $E_{\bar{\mathbf{q}}}$ as a function of G. As explained in the text, there exist nonzero values of G where the sloshing is strongly suppressed. Results for temperatures of $T = (0.125,\ 1,\ 8) \times \hbar\omega/k_B$ are plotted as dashed, full, and dotted lines, respectively.

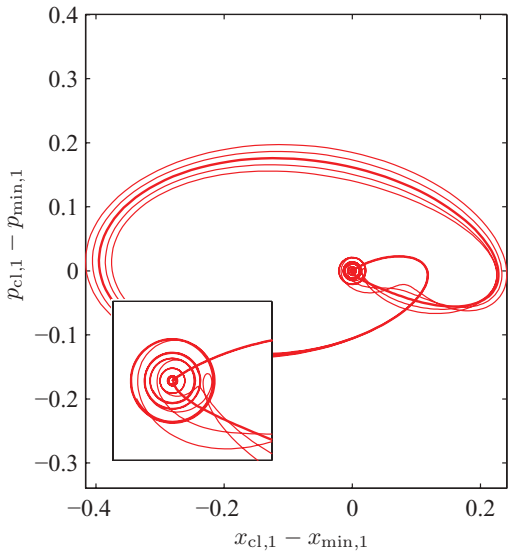

FIG. 3. (Color online) Phase-space trajectories for ion 1 for a push duration of $\omega\tau = 5.5$. The coordinates are relative to the potential minimum in which ion 1 is trapped. Perfect adiabatic evolution would correspond to the ion simply following this minimum, and thus the trajectory would be the single point (0,0) in this plot. Since the push is not infinitely slow, the ion will first lag behind the moving minimum and then oscillate in the moving potential. When the potential minimum again approaches its original position, the ion may happen to have just the right position and speed in order to end up at rest. Whether this is the case depends (for fixed push pulse) on G: The higher G is, the more the confinement is increased during the push. The thick line corresponds to $G = 0.002$, which is nearly optimal with respect to returning the ion to rest. The thin lines correspond to $G = 0$, 0.001, 0.003, and 0.004. The lowest G gives the outermost curve over the main part of the loop in the figure.

C. Sloshing errors

Let us now turn to the errors described by the $E_{\bar{\mathbf{q}}}$ term in Eq. (C8), the sloshing errors. Figure 2 shows how these errors are strongly dependent on G, the strength of the non-linearity of the pushing potential. A series of minima of $E_{\bar{\mathbf{q}}}$ as a function G can be seen. The optimal values of G depend on the chosen duration of the pulse, τ. Each minimum is associated with the ions performing an integer number of nonadiabatic oscillations during the push pulse. This is illustrated in Fig. 3, where the trajectory of ion 1 with respect to its trap minimum is plotted for values of G that are below, at, and above the one that leads to the lowest $E_{\bar{\mathbf{q}}}$.

In contrast to E_θ, $E_{\bar{\mathbf{q}}}$ depends noticeably on whether T is $(0.125,1,8) \times \hbar\omega/k_B$. Higher temperatures always increase the sloshing errors, and for $k_B T/\hbar\omega \gg 1$, we find that $E_{\bar{\mathbf{q}}}$ scales as T since γ does [see Eqs. (B21) and (B22)].

Curves for three different values of τ are plotted in Fig. 2, and it is immediately clear that one can dramatically decrease sloshing errors by making the gate slower and thus more adiabatic. The suppression of $E_{\bar{\mathbf{q}}}$ is exponential, and this is thus in general an efficient strategy.

D. Breathing errors

We now turn to the E_S term of Eq. (16). These breathing errors come from the different changes in the effective quadratic Hamiltonian for the different branches of the evolution. In Fig. 4, we plot E_S for different values of G and τ and for different temperatures of the external motion. Results for temperatures of $T = (0.125,1,8) \times \hbar\omega/k_B$ are shown, and it is first of all clear that E_S depends strongly on T. We also see that E_S is nearly proportional to $G^2\tau$. That larger G leads to larger errors is not surprising but that larger τ does is rather counterintuitive: Larger τ means a more smooth and thus more adiabatic push. It also means a smaller amplitude for the push since the ions will have more time to pick up the gate phase [cf. Eq. (27)]. Let us discuss the explanation for this behavior in more detail.

For exponential suppression of errors to be valid, the evolution should be well into the adiabatic regime. At first sight, the relevant time scale is ω^{-1}, the oscillation period of the microtraps. Since the traps are assumed to be far apart ($a_0 \ll d$), the parameter ϵ is small and the normal modes of the system have periods shifted little from this value: The CM mode is in fact unaffected by the Coulomb interaction and has frequency ω, while the relative motion mode oscillates at $\sqrt{1+\epsilon}\,\omega$. With $\omega\tau \gg 1$, one should therefore not be able to put excitations into either of these modes. However, it is perfectly possible to transfer excitations between the modes as the adiabatic time scale for this process is $(\sqrt{1+\epsilon}\,\omega - \omega)^{-1} \sim \epsilon^{-1}\omega^{-1}/2$. Such a transfer will be induced by mixing of the CM and relative motion during the gate operation. A linear push potential will not mix the two, but a nonlinear one will.

Another effect to remember is that when the instantaneous oscillation frequencies change during the push, the external motion will pick up different phases depending on the number

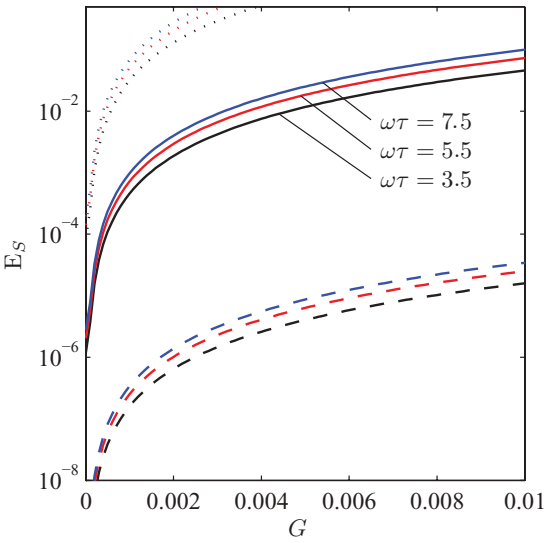

FIG. 4. (Color online) Breathing errors with nonuniform pushing forces. The physical parameters are $\epsilon = 0.04$, $a_0/d = 0.001$, and $\omega\tau = 3.5$ (black), 5.5 (red), and 7.5 (blue). Results for temperatures of $T = (0.125, 1, 8) \times \hbar\omega/k_B$ are plotted as dashed, full, and dotted lines, respectively. For all three temperatures, larger τ leads to larger E_S. E_S is increasing approximately linearly with $G^2\tau$; i.e., for fixed G, E_S will be proportional to τ, the pulse duration! This is very different from the behavior of $E_{\bar{q}}$ previously, which is rapidly decreased by increasing τ and thereby making the push more adiabatic.

of excitation quanta. Like the transfer of excitations, this effect, of course, disappears if the system is cooled to the ground state. A perturbative calculation to lowest order in a_0/d, G, and ϵ gives the result

$$E_S = \frac{\pi}{20} G^2 \xi^2 \omega^2 \tau^2 \times \left\{ \frac{1}{\sinh^2(\hbar\omega/2k_B T)} \left[1 + \exp\left(-\frac{\epsilon^2 \omega^2 \tau^2}{8} \right) \right] + 2 \left[\frac{1}{\sinh^2(\hbar\omega/2k_B T)} + 2 \right] \exp(-2\omega^2\tau^2) \right\}. \quad (28)$$

The prefactor gives the scaling behavior both in the naive nonadiabatic limit $\omega\tau < 1$ and in the more relevant intermediate region $1 < \omega\tau < \epsilon^{-1}$:

$$E_S \propto \xi^2 G^2 \omega^2 \tau^2 \propto \frac{G^2 \omega\tau}{\epsilon}. \quad (29)$$

In fact, even in the adiabatic limit $\epsilon\omega\tau \gg 1$, this scaling holds true since one term in Eq. (28) does not contain an exponential damping factor with τ^2. This unsuppressed term stems from the previously mentioned effect of time-varying instantaneous mode frequencies.

From Eq. (28), we can also understand the strong temperature dependence of the breathing errors. For $k_B T/\hbar\omega \gg 1$, the breathing errors will scale approximately like T^2. However, as seen in Fig. 4, high temperatures require very low values for G. For low temperatures, note that one term in Eq. (28) is not suppressed even at $T = 0$. This term stems from changes in the ground-state widths of the two instantaneous normal modes and is adiabatically suppressed when $\omega\tau \gg 1$. To find the dominant term for very low temperatures and short pulses, one should do a higher order perturbative calculation.

V. OPTIMIZING GATE PERFORMANCE

From the simulations in Sec. IV, we learn that without improvement, high fidelities require either very low values of G or cooling of the external motion almost to the ground state. In this section, we shall see how a better performance can be achieved by modifying the temporal shape of the push pulses.

A. Correcting the phase

Our first step will be to correct the gate phase by a simple scaling of the push pulse shape. From Fig. 1, we know that typical errors can be well above the percentage level. Our strategy is based on the observation that the simplest estimate of the gate phase suggests that it scales as the square of the push amplitude, ξ. [A general gate phase replaces the π in the numerator of Eq. (27).] We therefore divide ξ by the square root of the ratio of the observed gate phase and the ideal gate phase (π) and repeat the propagation. In Fig. 5, we show the results of applying this algorithm to the $\omega\tau = 7.5$ curves of Fig. 1. As can be seen, E_θ is rapidly reduced and can be brought below, for example, 10^{-6} in a very modest number of iterations. For simplicity, we ignore the temperature-dependent $\mathrm{Tr}[b\gamma]$ contribution to E_θ when rescaling the pulse. This is the reason for the $k_B T = 8\hbar\omega$ (dotted curves) departing from the $k_B T = 0.125\hbar\omega$ and $k_B T = 1\hbar\omega$ curves, especially at low G.

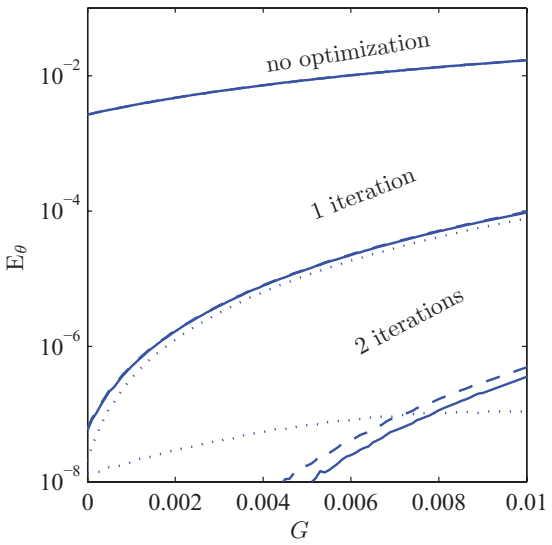

FIG. 5. (Color online) Improving E_θ by iteratively adjusting the push amplitude ξ. The pulse duration is $\omega\tau = 7.5$ and the other parameters are as in the previous figures. Four sets of curves are shown, each with results for $T = 0.125 \times \hbar\omega/k_B$ (dashed line), $1 \times \hbar\omega/k_B$ (solid line), and $8 \times \hbar\omega/k_B$ (dotted line). The uppermost set (looks like a single curve) is for the unoptimized pulse amplitude and is identical to the $\omega\tau = 7.5$ curves of Fig. 1. The progressively lower sets are for one and two iterations of the amplitude scaling described in the text. Note that as the error gets smaller, temperature begins to have an effect. This simple adjustment is capable of reducing E_θ below 10^{-6} for all the considered $G < 0.01$.

B. Fast gate: Eliminating sloshing in $\bar{x}$

A big advantage of the simple harmonic approximation is that it becomes feasible to solve the equations of motion many times with different temporal shapes of $f(t)$ in order to optimize the performance of the gate. Rather than simple trial and error, we will apply the global control algorithm of Krotov, which is guaranteed to improve the performance at each iteration [13–15]. The relevant equations for our case are given in Appendix C.

In general, it is desirable to complete the gate in as short a time as possible. This will limit many undesired effects and will ultimately enable faster quantum computations. A fast gate, however, means that the pushing force will deliver a rather abrupt impulse. This can lead to excitations of the external motion being left after the completion of the gate, limiting the fidelity. In this section, we show how such sloshing effects can be avoided by using optimal control.

We start from an initial Gaussian temporal shape of the push. The overall amplitude is first optimized iteratively to get the desired gate phase, as described earlier. We then run the Krotov algorithm to get a better shape of the pulse. We assume a nonuniform pushing force, $G = 2 \times 10^{-3}$. The result is plotted in Fig. 6. As can be seen, the influence of sloshing motion can be decreased by a couple orders of magnitude in a modest number of iterations.

To investigate the physical mechanism behind the reduction of the sloshing error, we plot in Fig. 7 (bottom) the difference between the optimized pulse $f_{\rm opt}(t)$ and the original Gaussian pulse $f_0(t) = \xi \exp(-t^2/\tau^2)$. This difference looks a lot like a simple cosine wave with a period close to $2\pi\omega^{-1}$ multiplied by a Gaussian of the same width as f_0. Thus the optimized pulse is approximately of the form

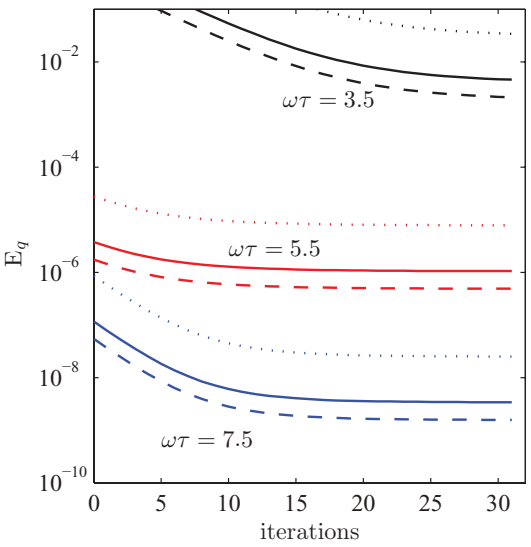

FIG. 6. (Color online) Optimization of pulse shape to eliminate sloshing. We plot $E_{\bar{q}}$, the contribution of sloshing to the total infidelity, as a function of the number of Krotov iterations performed. The parameters in this example are $\epsilon = 0.04$, $a_0/d = 0.001$, and $G = 2 \times 10^{-5}$. Each curve corresponds to a separate value of the pulse duration, $\omega\tau = (3.5, 5.5, 7.5)$, with larger τ always giving a lower value of $\mathcal{E}_{\bar{q}}$.

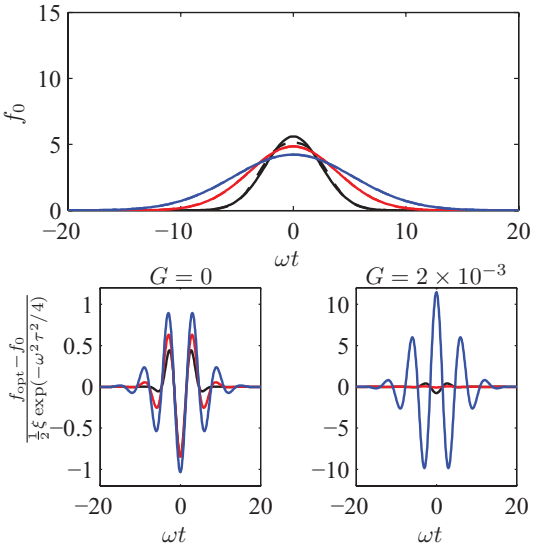

FIG. 7. (Color online) (top) Pulse shape both before (full line) and after (dashed line) Krotov optimization. Curves for three different pulse durations are shown: $\omega\tau = (3.5, 5.5, 7.5)$; other parameters are as in Fig. 6. Only for the shortest pulse is the optimized curve distinguishable from the original Gaussian. (bottom) Difference between optimized pulse and initial Gaussian pulse (after adjusting overall amplitude to reduce phase errors). The left plot is for $G = 0$, and the right plot is for $G = 2 \times 10^{-3}$. Each curve has been normalized to the prediction of a $G = 0$ perturbative calculation, which is seen to describe well the $G = 0$ case as all curves have a maximal excursion of approximately -1, while the $G \neq 0$ case is only qualitatively similar.

$f_{\rm opt}(t) \sim f_0(t) + A\cos(\omega t)\exp(-t^2/\tau^2)$. An approximative calculation of the sloshing excitation for the simplest $G = 0$ case reveals that for such a pulse, the nonresonant contribution of the bare Gaussian pulse is canceled by a resonant contribution from the cosine-modulated pulse. Since the resonant response is much stronger, only a small, negative A is needed for this cancellation. More precisely, the optimal A from first-order pertubation theory is given by $-\frac{1}{2}\xi\exp(-\omega^2\tau^2/4)$, and Fig. 7 shows that this is also what the Krotov algorithm converges to for $G = 0$. The strategy of the Krotov algorithm in this case seems therefore to be well understood. For $G \neq 0$, it is more difficult to predict the value of A, but nonetheless, the Krotov algorithm seems to be highly efficient.

C. Minimizing breathing errors

We now know that phase errors and sloshing errors can be controlled, and we turn to the breathing errors of Fig. 4. Without optimization, these errors put rather stringent limits on the parameters. In order to keep E_S at an acceptable level, either very low temperature or very small G is required. For very low temperature, $k_{\rm B}T = 0.125\hbar\omega$, we need just $G \lesssim 10^{-2}$ to get E_S below 10^{-4}, but if we assume a more modest cooling to $k_{\rm B}T = 1\hbar\omega$, the same error level requires $G \lesssim 2 \times 10^{-4}$. Note that even at $G = 0$, breathing errors persist, and that for $k_{\rm B}T = 8\hbar\omega$, they never get below the 10^{-5} level. These errors stem from the high-order terms in the Coulomb potential, which have been ignored in Eq. (28).

As described in Sec. IV D, breathing errors cannot be eliminated simply by increasing the push duration τ: First of all, the adiabatic time scale is $\sim \epsilon^{-1}\omega^{-1}/2$, which will mean a slow gate, and second, even in that limit, errors from the change in normal mode frequencies remain and even increase [compare the subsequent discussion and Eq. (29)]. It turns out that a simple application of the Krotov algorithm is also not very efficient in reducing the breathing errors. A partial explanation for this can be found from the perturbative calculation leading to Eq. (28) and the previous analysis of sloshing error reduction: Since the adiabatic time scale for the breathing errors is long, the Gaussian pulses we consider are not adiabatic with respect to breathing errors, and thus the admixture of a small resonant component in the push pulse will not be enough to get the cancellation we found in the case of sloshing errors. In fact, the amplitude of the cosine modulation should be comparable to the total amplitude for the relatively short pulses considered. There is nothing to be gained from a small-amplitude modulation, and thus the linear version of the Krotov algorithm we apply (see Appendix C) will not work.

In fact, in order to cancel out the contribution to the breathing errors because of mode frequency changes, sign changes in the push amplitudes are required during the pulse. This is beyond the simplest physical implementations, where the push amplitude is proportional to some laser intensity. In principle, it is possible to play with detunings to implement the sign changes, and this will in fact give many of the advantages of the π-pulse method (see Ref. [9]). Allowing negative push amplitudes and putting by hand an optimized $\cos(\epsilon\omega t/2)$ -modulated contribution, we have been able to, for example, reduce E_S below 10^{-6} for $\omega\tau = 7.5$, $G = 2 \times 10^{-3}$, and $T = 1 \times \hbar\omega/k_B$. Compared to the results reported in Fig. 4, this is a reduction by more than 3 orders of magnitude. Unfortunately, the strongly modified pulse now gives rise to large sloshing errors. To obtain an overall safisfactory fidelity, we use a combined strategy: We first put the breathing error reduction by hand, then iteratively reduce phase errors, and finally use the Krotov algorithm to reduce the sloshing errors. In Fig. 8, we show results of this strategy starting from $\omega\tau = 7.5$.

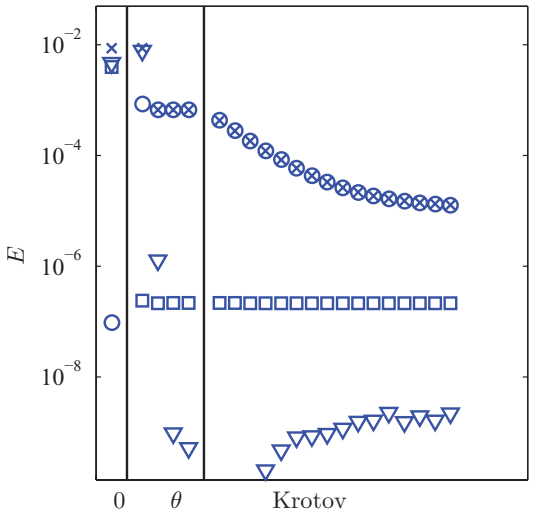

FIG. 8. (Color online) Combined strategy for reducing infidelity for $\epsilon = 0.04$ and $G = 2 \times 10^{-3}$. The three contributions E_θ, E_q, and E_S are labeled by triangles, circles, and squares, respectively. Their sum is labeled by crosses. The leftmost column contains the results for a simple Gaussian with $\omega\tau = 7.5$. The breathing errors dominate. In the next column, breathing errors have been reduced (but sloshing increased) by using a cosine-modulated pulse based on Eq. (28). The overall amplitude is then iteratively optimized to reduce phase errors, as described in Sec. V A. As can be seen, three iterations are more than sufficient to render E_θ completely insignificant. The dominating error type is now sloshing, and in the third column, the Krotov algorithm is applied to finally reduce the total infidelity below 10^{-4}.

VI. CONCLUSION

In this article, we have shown how a time-dependent, quadratic approximation to the Hamiltonian can be a useful tool when analyzing quantum gates based on conditional external dynamics. The resulting equations are much more manageable than the original two-body Schrödinger equations. This is especially true if one includes more spatial dimensions than the one considered here: A full time-dependent, three-dimensional, two-body wav function calculation is an extremely demanding numerical task, whereas the corresponding quadratic approximation will be much more manageable.

We used the developed method to show how to improve on a naive design of the pushing gate. This was done including a nonuniform contribution to the pushing force. An important lesson of our analysis and simulations is to pay attention to changes in the symmetry of the Hamiltonian during the gate operation. In the present case, a nonlinear push potential invalidates the separation of the dynamics into CM and relative motion. This opens up another type of nonadiabaticity, namely, transfer of excitations between the two normal modes. The adiabaticity parameter for this type of error is $\epsilon\omega\tau$, and for small ϵ, adiabaticity will require gate times much larger than the charateristic time of the microtraps. An efficient countermeasure is to decrease temperature so that there are in fact no excitations to transfer between modes. Failing that, one should increase ϵ as much as possible and, somewhat counterintuitively, do the gate as fast possible. Sloshing errors put a lower limit on the gate time, but as we show, an optimized choice of the temporal shape of the push can dramatically reduce this problem.

By analyzing the way that the Krotov optimized pulse reduces sloshing errors, we identified the basic mechanism as a destructive interference between the nonresonant, nonadiabatic contribution from the finite push pulse duration and a resonant contribution from a small-amplitude superposed oscillation of the push force. Generalizing this idea to deal with breathing errors, we were able to reduce them by several orders of magnitude. However, since breathing errors are not significantly adiabatically suppressed for the considered pulse durations, the destructive interference required sign changes in the push amplitude, which introduce experimental complications. The suppression of breathing errors also came at the price of increased sloshing errors, but we showed that the Krotov algorithm once again was able to improve the pulse shape.

One may ask to what extent the final pulse shape is optimal for the given overall gate time. This is an interesting question in general, and in this study, we saw examples both where the Krotov algorithm seemed to exhaust the potential in its strategy (the $G = 0$ case in Fig. 7) and where it was not able to find an optimization. In the latter case, we could improve the pulse by hand (eliminate the breathing errors by destructive interference). The problem of optimality is related to the question of a quantum speed limit (QSL) [16], and this connection has been studied in Ref. [17]. Note, however, that in our case, the Hamiltonian is time dependent, and what we want is in fact to leave the external motion unaffected after the pulse. It would be interesting to investigate such a general adiabaticity problem along the same lines as the work on the QSL.

ACKNOWLEDGMENTS

This research was supported in part by the National Science Foundation under Grant No. PHY05-51164 and in part by the EC projects AQUTE and EMALI.

APPENDIX A: EVOLUTION UNDER QUADRATIC HAMILTONIAN

In this appendix, we show that a second-order Hamiltonian leads to an evolution operator that can be written like $\hat{U}(t)$ [Eq. (12)]. For alternative parametrizations, see Refs. [18,19]. We will do a direct calculation showing that $\hat{U}(t)$ fulfills the Schrödinger equation:

$$i\frac{\partial}{\partial t}\hat{U} = \hat{H}_{\mathrm{so}}\hat{U}. \tag{A1}$$

The demanding part of the the calculation involves differentiating expontials of time-dependent operators. A useful formula can be found in, for example, Ref. [20] and involves integration over an auxillary variable η. It results in

$$\begin{aligned} i\frac{\partial}{\partial t}\hat{D}_{\mathbf{c}} &= \int_0^1 \hat{D}_{\eta\mathbf{c}}\ \dot{\mathbf{c}}^{\mathrm{T}} J\hat{\mathbf{q}}\ \hat{D}_{\eta\mathbf{c}}^{\dagger}\, d\eta\ \hat{D}_{\mathbf{c}} \\ &= \int_0^1 \dot{\mathbf{c}}^{\mathrm{T}} J\,(\hat{\mathbf{q}} - \eta\mathbf{c})\ d\eta\ \hat{D}_{\mathbf{c}} \\ &= \dot{\mathbf{c}}^{\mathrm{T}} J\left(\hat{\mathbf{q}} - \frac{1}{2}\mathbf{c}\right)\hat{D}_{\mathbf{c}} \end{aligned} \tag{A2}$$

for the displacement operator and

$$\begin{aligned} i\frac{\partial}{\partial t}\hat{W}_b &= \int_0^1 \hat{W}_{\eta b}\,\frac{1}{2}\hat{\mathbf{q}}^{\mathrm{T}}\dot{b}\hat{\mathbf{q}}\hat{W}_{\eta b}^{\dagger}\, d\eta\ \hat{W}_b \\ &= \frac{1}{2}\int_0^1 (e^{-\eta Jb}\hat{\mathbf{q}})^{\mathrm{T}}\dot{b}(e^{-\eta Jb}\hat{\mathbf{q}})\, d\eta\ \hat{W}_b \\ &= \frac{1}{2}\hat{\mathbf{q}}^{\mathrm{T}}J^{\mathrm{T}}\int_0^1 e^{\eta Jb}J\dot{b}e^{-\eta Jb}\, d\eta\ \hat{\mathbf{q}}\hat{W}_b \\ &= \frac{1}{2}\hat{\mathbf{q}}^{\mathrm{T}}J^{\mathrm{T}}\left(\frac{\partial}{\partial t}e^{Jb}\right)e^{-Jb}\ \hat{\mathbf{q}}\ \hat{W}_b \end{aligned} \tag{A3}$$

for the squeezing operator. It is now easy to show that the equations of motion (14) for ϕ, $\mathbf{c}$, and $S = \exp(Jb)$ lead to $\hat{U} = \exp(-i\phi)\hat{D}_{\mathbf{c}}\hat{W}_b$, fulfilling Eq. (A1).[3]

APPENDIX B: FIDELITY FOR GAUSSIAN EVOLUTIONS

In this section, we derive expressions for the fidelity as a function of the variables used to characterize the evolution in the harmonic approximation, ϕ_β, $\bar{\mathbf{q}}_\beta$, and S_β, $\beta = 00,01,10,11$.

If we assume that the initial state of the system is a product of an internal state density matrix and an external state density matrix, $\rho\otimes\sigma$, we get the following state for the internal degrees of freedom after the application of $\hat{U}^{\mathrm{tot}}$ of Eq. (2):

$$\begin{aligned} \rho' &= \mathrm{Tr}_{\mathrm{ex}}[\hat{U}^{\mathrm{tot}}\rho\otimes\sigma(\hat{U}^{\mathrm{tot}})^{\dagger}] \\ &= \sum_{\alpha\beta}|\alpha\rangle\langle\beta|\ [\rho\circ R]_{\alpha\beta}. \end{aligned} \tag{B1}$$

Here $\circ$ denotes the elementwise matrix product (the Hadamard product) and R is the matrix given by

$$[R]_{\alpha\beta} = \mathrm{Tr}\big[\hat{U}_{\alpha}^{\mathrm{ex}}\sigma\left(\hat{U}_{\beta}^{\mathrm{ex}}\right)^{\dagger}\big]. \tag{B2}$$

It is easy to see that R is Hermitian and that all its diagonal elements are 1. In particular, $\mathrm{Tr}R = 4$. Slightly less obvious is that R is positive semidefinite: Let $c\in\mathbb{C}^4$. Then

$$\begin{aligned} c^{\dagger}Rc &= \mathrm{Tr}\Big[\Big\{\sum c_{\alpha}^{*}\hat{U}_{\alpha}^{\mathrm{ex}}\Big\}\sigma\Big\{\sum c_{\beta}\big(\hat{U}_{\beta}^{\mathrm{ex}}\big)^{\dagger}\Big\}\Big] \\ &= \mathrm{Tr}\Big[\Big\{\sum c_{\beta}^{*}\hat{U}_{\beta}^{\mathrm{ex}}\Big\}^{\dagger}\Big\{\sum c_{\alpha}^{*}\hat{U}_{\alpha}^{\mathrm{ex}}\Big\}\sigma\Big] \geqslant 0, \end{aligned} \tag{B3}$$

where we have used the cyclic property of the trace and the fact that the trace of a product of positive semidefinite operators is nonnegative.

The elementwise product form in Eq. (B1) is perhaps not the most illuminating. If we diagonalize $R = \sum_h w_h w_h^{\dagger}$, we get instead a Krauss operator sum form

$$\rho' = \sum_{h=1}^{4} K_h\rho K_h^{\dagger}, \tag{B4}$$

with $K_h = \mathrm{diag}(w_h)$.

There are different ways to define the fidelity of the gate. The one used in Refs. [8,9] is the minimum fidelity of the obtained final state with respect to the wanted final state when the input state is varied. This means that

$$F_{\mathrm{min}} = \min_{\psi}\langle\psi|U_0^{\dagger}\rho'_{\psi}U_0|\psi\rangle, \tag{B5}$$

[3]There are two caveats regarding the equation of motion for S. First of all, the translation from S to b and thus $\hat{W}_b$ is not one to one. Second, the equation of motion for S cannot necessarily be fulfilled by an S in the form $\exp(Jb)$ with a differentiable $b(t)$. Both problems are, however, eliminated when the Ss in the four branches never deviate much from each other.

with $\rho_\psi = |\psi\rangle\langle\psi|$ and U_0 being the gate operator we aim for. In the case of a phase gate, U_0 is diagonal in the logical state basis:

$$\hat{U}_0 = \sum_\beta |\beta\rangle\langle\beta| e^{i\theta_\beta}, \tag{B6}$$

and we get the simpler minimization problem

$$F_{\min} = \min_{\{p_i\}} p^{\mathrm{T}} \tilde{R} p, \tag{B7}$$

where the $p \in \mathbb{R}_+^4$ and $\sum p_i = 1$. The matrix $\tilde{R} = U_0 R U_0^\dagger$ is Hermitian, but since p is confined to be real, only its real symmetric part contributes. The minimization in Eq. (B7) is a so-called quadratic programming problem, and very efficient numerical methods for its solution exist. Given $\tilde{R}$, it is therefore simple to calculate $F_{\min}$ on the computer. However, a more direct evaluation is possible if fidelity is instead defined as an average over input states as

$$F_{\mathrm{av}} = \int_{S^{2n-1}} \langle\psi|U_0^\dagger \rho'_\psi U_0|\psi\rangle \, dV. \tag{B8}$$

Here S^{2n-1} denotes the normalized states (unit sphere) in $\mathbb{C}^n$, and the volume element dV is such that $\int_{S^{2n-1}} dV = 1$. For F_{av}, a compact formula exists [21], and using it in the present case leads to

$$F_{\mathrm{av}} = \frac{1}{4(4+1)} \left(\mathrm{Tr}\tilde{R} + \sum_{\alpha\beta} \tilde{R}_{\alpha\beta} \right), \tag{B9}$$

or when using the properties of $\tilde{R}$,

$$1 - F_{\mathrm{av}} = \frac{1}{10} \sum_{\alpha<\beta} [1 - \mathrm{Re}(\tilde{R}_{\alpha\beta})]. \tag{B10}$$

1. General small errors

Typically, we will be mostly interested in situations where the four logical states lead to almost identical evolutions for the external states. It is then useful to write

$$\begin{aligned} \hat{U}_\beta^{\mathrm{ex}} &= \exp(i\hat{D}_\beta)\hat{U}_{\mathrm{com}}^{\mathrm{ex}} \\ &= \exp(i\langle\hat{D}_\beta\rangle)\exp(i\Delta\hat{D}_\beta)\hat{U}_{\mathrm{com}}^{\mathrm{ex}}, \end{aligned} \tag{B11}$$

where $\langle\hat{D}\rangle = \mathrm{Tr}[\hat{D}\hat{U}_{\mathrm{com}}^{\mathrm{ex}}\sigma_{\mathrm{ex}}(\hat{U}_{\mathrm{com}}^{\mathrm{ex}})^\dagger]$ and $\Delta\hat{D} = \hat{D} - \langle\hat{D}\rangle$. Calculating $\tilde{R}$ to second order in the $\Delta\hat{D}$s, we get

$$\begin{aligned} \tilde{R}_{\alpha\beta} = \exp(i\Delta\theta_\alpha)\{1 - \tfrac{1}{2}\langle\Delta\hat{D}_\alpha^2 + \Delta\hat{D}_\beta^2 - 2\Delta\hat{D}_\alpha\Delta\hat{D}_\beta\rangle\} \\ \times \exp(-i\Delta\theta_\beta). \end{aligned} \tag{B12}$$

This form is useful as it separates the infidelity into systematic phase errors [the $\exp(\pm i\Delta\theta_\alpha)$ factors] and decoherence (factor in curly brackets). The phase errors $\Delta\theta_\beta = \langle\hat{D}_\beta\rangle - \theta_\beta$ can be made small by tuning the average of laser powers, and this can usually be done very well. The challenge will therefore most often be to suppress the fluctuations, that is, the terms in curly brackets in Eq. (B12).

Assuming also the $\Delta\theta$s to be small, Eq. (B10) becomes

$$1 - F_{\mathrm{av}} = \frac{1}{20} \sum_{\alpha<\beta} \{[\Delta\theta_\alpha - \Delta\theta_\beta]^2 + \langle(\Delta\hat{D}_\alpha - \Delta\hat{D}_\beta)^2\rangle\}. \tag{B13}$$

At first sight, this form might seem dubious since only differences in the $\Delta\theta$s and $\Delta\hat{D}$s enter. However, one should remember that any common evolution on the four branches can be absorbed into $\hat{U}_{\mathrm{com}}^{\mathrm{ex}}$ in Eq. (B11). This emphasizes that for the implementation of a single gate on the logical state, the external motion must not necessarily be returned to its initial state as long as the final state is common to all logical input states. Typically, the further requirement that energy not be pumped into the external degrees of freedom by repeated application of the gate must be made. In the particular case of the pushing gate, this requirement is in fact already hidden in Eq. (B13) since the $\beta = 00$ branch contains no pushing. In other cases, one could apply cooling to the external state between gate operations.

2. The nonlocal part of the phase

We are seeking to implement the phase gate (B6). In many cases, the θ_βs are not so important individually since single-particle operations are easy to perform and only the truely nonlocal phase is interesting. Assuming that perfect single-particle phase changes can be implemented on average, it is straightforward to show that one should replace $\sum_{\alpha<\beta}[\Delta\theta_\alpha - \Delta\theta_\beta]^2$ by

$$[\Delta\theta_{00} - \Delta\theta_{01} - \Delta\theta_{10} + \Delta\theta_{11}]^2 \tag{B14}$$

in Eq. (B13).

This simplified view of single-particle phase changes should of course be revisited in a more complete analysis of any given proposal for quantum computing. In the present work, we use the replacement (B14) throughout, but let us emphasize that fluctuations in the single-particle phase rotations are more naturally incorporated in the $\Delta\hat{D}$ terms of Eq. (B13) than in the $\Delta\theta$ terms: One simply models the fluctations as a consequence of some fluctuating parameter which can be included in σ_{ex}.

3. The Gaussian case

For Gaussian evolutions like Eq. (12) and a Gaussian (e.g., thermal) external state σ with covariance matrix

$$\begin{aligned} \gamma_{ij} &= \tfrac{1}{2}\langle q_i q_j + q_j q_i\rangle - \langle q_i\rangle\langle q_j\rangle \\ &= \mathrm{ReTr}[q_i q_j \sigma] - \mathrm{Tr}[q_i\sigma]\mathrm{Tr}[q_j\sigma] \end{aligned} \tag{B15}$$

and vanishing means

$$\langle q_i\rangle = \mathrm{Tr}\,[q_i\sigma] = 0, \tag{B16}$$

one gets phase contributions

$$\langle\hat{D}_\beta\rangle = -\phi_\beta - \mathrm{Tr}[b_\beta\gamma] \tag{B17}$$

and decoherence terms

$$\begin{aligned} \langle(\Delta D_\alpha - \Delta D_\beta)^2\rangle = (c_\alpha - c_\beta)^{\mathrm{T}} J\gamma J^{\mathrm{T}}(c_\alpha - c_\beta) \\ + \tfrac{1}{2}\mathrm{Tr}[(b_\alpha - b_\beta)\gamma(b_\alpha - b_\beta)\gamma] \\ + \tfrac{1}{8}\mathrm{Tr}[(b_\alpha - b_\beta)J(b_\alpha - b_\beta)J]. \end{aligned} \tag{B18}$$

In general, for a harmonic oscillator in thermal equilibrium at temperature T, the covariance matrix is given by

$$\gamma_{\text{thermal}} = \frac{1}{2}\frac{1}{\tanh\frac{\hbar\omega}{2k_BT}}\begin{bmatrix}\frac{\hbar}{m\omega} & 0\\ 0 & \hbar m\omega\end{bmatrix}, \tag{B19}$$

where k_B is the Boltzmann constant. In the present case, the CM and the relative motion are separately in thermal equilibrium, and for the corresponding dimensionless position and momentum operators [$x_{\text{CM}} = (x_1 + x_2)/2$, etc.], we get

$$\gamma = \gamma_{\text{CM}} \oplus \gamma_{\text{rel}}, \tag{B20}$$

with

$$\gamma_{\text{rel}} = \frac{1}{2}\frac{1}{\tanh\frac{(1+\epsilon)^{1/2}\hbar\omega}{2k_BT}}\begin{bmatrix}\frac{2}{(1+\epsilon)^{1/2}} & 0\\ 0 & \frac{(1+\epsilon)^{1/2}}{2}\end{bmatrix} \tag{B21}$$

and

$$\gamma_{\text{CM}} = \frac{1}{2}\frac{1}{\tanh\frac{\hbar\omega}{2k_BT}}\begin{bmatrix}\frac{1}{2} & 0\\ 0 & 2\end{bmatrix}. \tag{B22}$$

In the limit $\epsilon \ll 1$, we have approximately $\gamma \propto \mathbb{I}_4$ if we use the set of individual ion operators (x_1, x_2, p_1, p_2).

APPENDIX C: THE KROTOV ALGORITHM

Optimizing the temporal shape of the push pulse is done using the Krotov algorithm [13]. For an introduction to the method, see, for example, Ref. [14].

1. Auxillary variables

The key ingredient in this approach is a function $\Phi(t, \{\phi_\beta, \bar{\mathbf{q}}_\beta, S_\beta\}_{\beta=00,01,10,11})$ which allows us to translate the global goal of improving the final $\hat{U}^{\text{tot}}(T)$ to a local problem of choosing a better $f(t)$ for each t. Constructing Φ is in general very difficult, but it is relatively simple to get a linear approximation to it. The coefficients in this approximation will constitute a set of auxillary variables. For each branch, the equations of motion for the auxillary variables $\tilde{\phi}_\beta$, $\tilde{\mathbf{q}}_\beta$, and $\tilde{S}_\beta$ are determined by the requirement that they are conjugate to the physical variables ϕ_β, $\bar{\mathbf{q}}_\beta$, and S_β, respectively.

Let us focus on a single branch and suppres the β index like in Sec. II A. We then need to construct $\mathcal{H}(t; \phi, \bar{\mathbf{q}}, S; \tilde{\phi}, \tilde{\mathbf{q}}, \tilde{S})$ such that Eqs. (14) can be written

$$\frac{\partial}{\partial t}\phi = \frac{\partial}{\partial\tilde{\phi}}\mathcal{H}, \tag{C1}$$

$$\frac{\partial}{\partial t}\bar{q}_i = \frac{\partial}{\partial\tilde{q}_i}\mathcal{H}, \tag{C2}$$

$$\frac{\partial}{\partial t}S_{ij} = \frac{\partial}{\partial\tilde{S}_{ij}}\mathcal{H}. \tag{C3}$$

This leads simply to

$$\begin{aligned}\mathcal{H}(t; \phi, \bar{\mathbf{q}}, S; \tilde{\phi}, \tilde{\mathbf{q}}, \tilde{S}) = {}& \tilde{\phi}\left[E(t, \bar{\mathbf{x}}) - \tfrac{1}{2}\mathbf{F}^{\mathrm{T}}(t, \bar{\mathbf{x}})\right]\\ & + \tilde{\mathbf{q}}^{\mathrm{T}}[Jh(t, \bar{\mathbf{x}})\bar{\mathbf{q}} - J\mathbf{F}(t, \bar{\mathbf{x}})]\\ & + \mathrm{Tr}[\tilde{S}^{\mathrm{T}}Jh(t, \bar{\mathbf{x}})S].\end{aligned} \tag{C4}$$

Then the equations of motion for the auxillary variables become

$$\frac{\partial}{\partial t}\tilde{\phi} = -\frac{\partial}{\partial\phi}\mathcal{H} = 0, \tag{C5}$$

$$\frac{\partial}{\partial t}\tilde{\mathbf{q}} = -\nabla_{\bar{\mathbf{q}}}\mathcal{H}, \tag{C6}$$

$$\frac{\partial}{\partial t}\tilde{S} = \nabla_S\mathcal{H} = h(t, \bar{\mathbf{x}})J\tilde{S}. \tag{C7}$$

The equation of motion for $\tilde{\mathbf{q}}$ is rather involved since $\mathcal{H}$ depends on $\bar{\mathbf{x}}$ in a complicated manner through h, F, and E. It can be rewritten as two coupled time-dependent, forced harmonic oscillators. Note, on the other hand, that $\tilde{\phi}$ is time independent and that $J\tilde{S}$ solves the same equation as S.

2. Objective function

Our ultimate goal is to improve the fidelity of the gate. However, it is somewhat impractical to apply this as the objective in the Krotov algorithm: Calculating the fidelity is only simple for small errors, and in general, it depends on, for example, the temperature of the external motion. Instead we shall work with a simpler function of the variables ϕ, $\bar{\mathbf{q}}$, and S for the four branches. The reduction of this objective function should tend to increase the fidelity of the gate. On the basis of the fact that in the pushing gate, the branch $\beta = 00$ is not subject to any time-dependent forces, we choose the following:

$$\begin{aligned}&\mathcal{J}(\{\phi_\beta, \bar{\mathbf{q}}_\beta, S_\beta\}_{\beta=00,01,10,11})\\ &\quad = \mathcal{J}_\phi + \mathcal{J}_q + \mathcal{J}_S\\ &\quad = \frac{1}{2}[\phi_{00} - \phi_{01} - \phi_{10} + \phi_{11} - \pi]^2\\ &\qquad + \frac{1}{2}\sum_\beta[(\mathbf{x}_\beta - \mathbf{x}_{00})^2 + (\mathbf{p}_\beta - \mathbf{p}_{00})^2]\\ &\qquad + \frac{1}{2}\sum_\beta \mathrm{Tr}[(S_\beta - S_{00})^{\mathrm{T}}(S_\beta - S_{00})].\end{aligned} \tag{C8}$$

The term with ϕs aims to ensure the correct phase in the phase gate, while the other terms aim at identical evolution for the external motion in the four branches. In the limit $\epsilon \ll 1$, Eq. (B13) formally justifies the use of our chosen objective function, given the extra proviso that we are only interested in the nonlocal part of the phase.

3. Terminal conditions

The objective function supplements the auxillary-variable equations of motion (C5)–(C7) with the following terminal conditions, that is, boundary conditions at $t = T$:

$$\begin{aligned}\tilde{\phi}_\beta(T) &= -\frac{\partial}{\partial\phi_\beta}\mathcal{J}\Big|_T\\ &= -(-1)^\beta(\phi_{00} - \phi_{01} - \phi_{10} + \phi_{11} - \pi)|_T,\end{aligned} \tag{C9}$$

$$\tilde{\mathbf{x}}_\beta(T) = -\nabla_{\bar{\mathbf{x}}_\beta}\mathcal{J}|_T = \begin{cases} -(3\bar{\mathbf{x}}_{00} - \bar{\mathbf{x}}_{01} - \bar{\mathbf{x}}_{10} - \bar{\mathbf{x}}_{11})|_T, & \beta = 00, \\ -(\bar{\mathbf{x}}_\beta - \bar{\mathbf{x}}_{00})|_T, & \beta \neq 00, \end{cases} \tag{C10}$$

$$\tilde{\mathbf{p}}_\beta(T) = -\nabla_{\bar{\mathbf{p}}_\beta}\mathcal{J}|_T = \begin{cases} -(3\bar{\mathbf{p}}_{00} - \bar{\mathbf{p}}_{01} - \bar{\mathbf{p}}_{10} - \bar{\mathbf{p}}_{11})|_T, & \beta = 00, \\ -(\bar{\mathbf{p}}_\beta - \bar{\mathbf{p}}_{00})|_T, & \beta \neq 00, \end{cases} \tag{C11}$$

$$\tilde{S}_\beta(T) = -\nabla_{S_\beta}\mathcal{J}|_T = \begin{cases} -(3S_{00} - S_{01} - S_{10} - S_{11})|_T, & \beta = 00, \\ -(S_\beta - S_{00})|_T, & \beta \neq 00, \end{cases} \tag{C12}$$

where $(-1)^\beta$ is $+1$ for $\beta = 00$ and 11 and -1 for $\beta = 01$ and 10. These equations express the values of the auxillary varibles at time $t = T$ in terms of the physical variables also at $t = T$ and give the input to the backward propagation of the auxillary variables (cf. Ref. [13]).

[1] J. I. Cirac and P. Zoller, Phys. Rev. Lett. **74**, 4091 (1995).
[2] J. I. Cirac and P. Zoller, Nature (London) **404**, 579 (2000).
[3] D. Jaksch, H.-J. Briegel, J. I. Cirac, C. W. Gardiner, and P. Zoller, Phys. Rev. Lett. **82**, 1975 (1999).
[4] T. Calarco, E. A. Hinds, D. Jaksch, J. Schmiedmayer, J. I. Cirac, and P. Zoller, Phys. Rev. A **61**, 022304 (2000).
[5] G. Burkard, D. Loss, and D. P. DiVincenzo, Phys. Rev. B **59**, 2070 (1999).
[6] D. P. DiVincenzo, Fortschr. Phys. **48**, 771 (2000).
[7] D. D'Alessandro, *Introduction to Quantum Control and Dynamics* (Chapman and Hall/CRC, Boca Raton, 2008).
[8] T. Calarco, J. I. Cirac, and P. Zoller, Phys. Rev. A **63**, 062304 (2001).
[9] M. Šašura and A. M. Steane, Phys. Rev. A **67**, 062318 (2003).
[10] R. G. Littlejohn, Phys. Rep. **138**, 193 (1986).
[11] H. Häffner, S. Gulde, M. Riebe, G. Lancaster, C. Becher, J. Eschner, F. Schmidt-Kaler, and R. Blatt, Phys. Rev. Lett. **90**, 143602 (2003).
[12] A. Kaplan, M. F. Andersen, and N. Davidson, Phys. Rev. A **66**, 045401 (2002).
[13] V. F. Krotov, *Global Methods in Optimal Control Theory* (Marcel Dekker, New York, 1995).
[14] S. E. Sklarz and D. J. Tannor, Phys. Rev. A **66**, 053619 (2002).
[15] D. Tannor, V. Kazakov, and V. Orlov, in *Time Dependent Quantum Molecular Dynamics*, edited by J. Broeckhove and L. Lathouwers (Plenum, New York, 1992), p. 347.
[16] V. Giovannetti, S. Lloyd, and L. Maccone, Phys. Rev. A **67**, 052109 (2003).
[17] T. Caneva, M. Murphy, T. Calarco, R. Fazio, S. Montangero, V. Giovannetti, and G. E. Santoro, Phys. Rev. Lett. **103**, 240501 (2009).
[18] R. Gilmore and J.-M. Yuan, J. Chem. Phys. **86**, 130 (1987).
[19] R. Gilmore and J.-M. Yuan, J. Chem. Phys. **91**, 917 (1989).
[20] R. M. Wilcox, J. Math. Phys. **8**, 962 (1967).
[21] L. H. Pedersen, N. M. Møller, and K. Mølmer, Phys. Lett. A **367**, 47 (2007).